# MEASUREMENT AND UNCERTAINTY EVALUATION OF INNER DIAMETER AND ROUNDNESS BY PNEUMATIC METHOD USED FOR INDUSTRIAL SITE

Tingting ZHANG[1], Chuanzhi FANG[2*], Zongjun YIN[3*], Rong SU[4], Jiaqian ZHA[5], Biyun TAO[6]

*The inner diameter and roundness of precision parts are crucial parameters that significantly impact product accuracy. The pneumatic method, based on the principle of pressure difference, offers a cost-effective solution for achieving stable high-precision at the micrometer level and holds substantial value in the manufacturing environment. When measuring inside a hole using a cylindrical commercial pneumatic probe, strict alignment of the measurement line center with the measured inner hole center is challenging, leading to radial error. This error exhibits randomness and follows the uniform distribution, but quantifying distribution parameters poses difficulties. According to the central extreme value theorem, a three-position measurement method for a CNC machined part is devised and the radial error distribution is transformed. By using the Monte Carlo Method (MCM), the evaluation of measurement uncertainty is conducted. The experimental results indicate that the result of the measuring inner diameter is 25.0118 mm with an extended uncertainty (k=2) of 0.22 μm, and the roundness is 7.10 μm with an extended (k=2) uncertainty of 0.64 μm, providing more reliable measurement output for the inner hole parameters.*

**Keywords:** roundness; Monte Carlo method; measurement error; uncertainty

## 1. Introduction

In the field of advanced manufacturing, the roundness of precise hole-shaped components significantly impacts the assembly accuracy of precision machinery. Measuring and evaluating uncertainties of diameter and roundness are

[1] School of Mechanical Engineering, Anhui Institute of Information Technology, Wuhu 241100, China; email: zhtt1126@163.com
[2] School of Mechanical Engineering, Anhui Institute of Information Technology, Wuhu 241100, China; email: fangchuanz@163.com
[3] School of Mechanical Engineering, Anhui Institute of Information Technology, Wuhu 241100, China; email: yinzongjunyzj@163.com
[4] School of Mechanical Engineering, Anhui Institute of Information Technology, Wuhu 241100, China; email: 197625962@qq.com
[5] School of Mechanical Engineering, Anhui Institute of Information Technology, Wuhu 241100, China; e-mail: 1959742926@qq.com
[6] School of Mechanical Engineering, Anhui Institute of Information Technology, Wuhu 241100, China; e-mail: 3327679607@qq.com
* Corresponding authors: Chuanzhi Fang, Email: fangchuanz@163.com; Zong-jun Yin, Email: yinzongjunyzj@163.com

crucial methodologies for ensuring precision assembly processing. Numerous research achievements have been accumulated in this area, encompassing diverse characteristics that have been investigated to measure the inner diameter and roundness of hole-shaped components. Coordinate measuring machines (CMMs) are widely used instruments for precise measurement at the micrometer level [1,2], particularly suitable for large-sized parts. However, CMMs impose stringent environmental control requirements [3] and entail high costs, posing challenges in meeting the demands of rapid measurements in industrial settings. The articulated three-coordinate system [4,5] commonly employed in industrial field measurement exhibits relatively low accuracy and remains costly. Machine vision methods possess the advantages of rapid and non-destructive testing [6,7]. However, they are significantly influenced by lighting conditions and typically limited to planar measurements [8], thereby posing challenges for depth measurement of features within holes. Achieving depth measurement through three-dimensional visual operations is demanding and expensive [9,10], often necessitating complex sub-pixel edge detection algorithms to achieve sub-micron-level resolution [11,12].

The pneumatic measurement method [13] utilizes the principle of pressure difference to achieve high-precision measurement and robust anti-interference ability under stable gas quality and pressure. Customized commercial pneumatic measurement instruments have been developed for different morphologies. For internal diameter measurement using pneumatic instrument, a cylindrical pneumatic probe is inserted into the hole to generate a pressure difference based on the shape of the hole, which is then converted into displacement output. However, a principle error occurs in the radial direction caused by the non-coincidence of the measurement line center and the hole center. The error exhibits randomness and follows the uniform distribution, but quantifying distribution parameters poses difficulties. This study aims to address this issue by proposing a method for measuring inner diameter and roundness based on commercial pneumatic probe. A three-position measurement methodology for a CNC machined part is devised and the radial error distribution is transformed according to the central extreme value theorem. In addition, the uncertainty is evaluated by using Monte Carlo method (MCM) [14-16]. These efforts further ensure measurement accuracy, providing a foundation for rapid and high-precision measurement of inner hole parameters in industrial settings.

## 2. Error analysis of pneumatic inner hole measurement

Pneumatic displacement measurement is mainly based on gas flow pressure difference, and its principle is shown in Fig. 1.

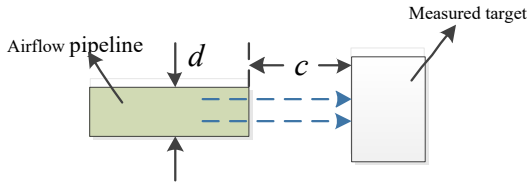


Fig. 1. Principle of Pneumatic Displacement Measurement

The diameter of the airflow pipeline in Figure 1 is $d$, and the distance between the pipeline outlet and the target object is $c$. When the air pressure is large enough and $c$ is small, the shape of the gas flowing out of the pipeline between the pipeline and the target object is a cylinder. The relationship between the gas flow rate $K$ and the side area of the cylinder is shown in Equation (1).

$$K = f(\pi dc) \tag{1}$$

When $d$ is constant, $K$ is only related to $c$. The displacement $c$ can be obtained by comparing the pressure difference. For a commercial instrument, the conversion structure between $K$ and $c$ is integrated inside the device, and the displacement data is automatically output from the customized probe based on the shape of the part.

The installation structure for measuring the inner hole of a commercial pneumatic instrument is shown in Fig. 2.

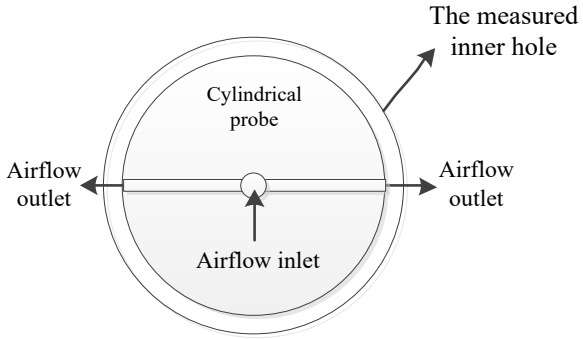


Fig. 2. Schematic diagram of measuring inner hole with a commercial measuring instrument

The inner hole measuring probe is a cylindrical body that goes deep into the measured hole for measurement. A radial through-hole is opened at the center of the measuring probe as the airflow outlet, and the two airflow outlets form a differential structure at symmetrical positions to improve measurement accuracy. Given the influence of roundness error, a single direction measurement value is insufficient to characterize the part's inner diameter. Therefore, the inner diameter results from multiple angles around the circumference must be comprehensively measured, as shown in Fig. 3.

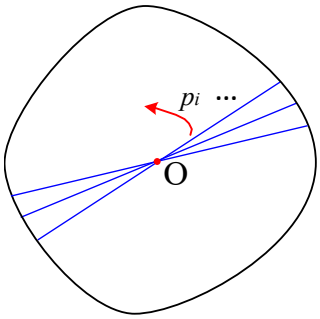


Fig. 3. Schematic diagram of inner hole measurement

Let $p_i$ ($i$=1,2,..., n) be the inner diameter measurement values at different angles around the circumference. According to the principle of least squares, if the angle intervals at each measurement position are equal and the measurement line passes through the center of the least squares circle O, then the inner diameter $D$ and roundness $\Delta$ of the part can be obtained from Equations (2) and (3), respectively.

$$D = \frac{1}{n}\sum_{i=1}^{n}\left(p_i\right) \tag{2}$$

$$\Delta = max(\frac{p_i}{2}) - min(\frac{p_i}{2}) \tag{3}$$

Characterizing the diameter and roundness of the inner hole using the above principle has a prerequisite. In the radial direction, the center of the circumference chord in the direction of the measuring line (airflow outlet direction) of the probe should coincide with the least squares center of the part's circular contour. In the actual measurement, given the randomness of the measurement position of the probe entering the hole, the above situation is challenging to achieve, and the error analysis is shown in Fig. 4.

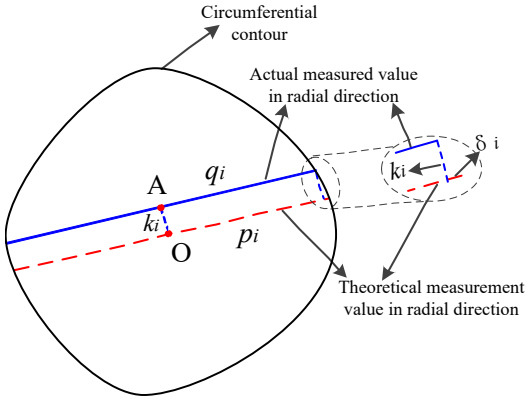


Fig. 4. Schematic diagram of radial error of inner hole measurement

The O point is the center of the least squares circle, and the theoretical measurement line length that passes through the O point radially is $p_i$. $q_i$ is the actual measurement value, A is the midpoint of the actual measurement line segment, $k_i$ is the distance between the two points in OA, and the radial measurement error caused by $k_i$ is $\delta_i$ along the measurement direction. The details of the error are partially enlarged for easier understanding in the figure. Therefore, the single-point measurement value after principle error correction [17] is

$$p_i = q_i + \delta_i \tag{4}$$

The inner diameter value is

$$D = \frac{1}{n}\sum_{i=1}^{n}\left(q_i + \delta_i\right) \tag{5}$$

The roundness is

$$\Delta = max(\frac{q_i + \delta_i}{2}) - min(\frac{q_i + \delta_i}{2}) \tag{6}$$

When measuring the same circumference at different positions, the value of $k_i$ in Figure 4 is difficult to determine, but the probability of taking any value between 0 and max ($k_i$) is equal, indicating the uniform distribution. Thus, the radial error $\delta_i$ caused by $k_i$ can be any value between 0 and max($\delta_i$), but the upper limit of the uniform distribution is difficult to determine.

According to the central extreme value theorem, the sum of multiple sequences uniformly distributed will gradually approach normal distribution with increasing the number of sequences. When the values of uniform distribution of each sequence are similar, the sum of three or more uniform sequences is an approximately normal distribution. Therefore, a three-position inner hole measurement method is designed to measure different positions at multiple angles. The normal distribution of the overall sample can be determined by summing the samples from three groups, and the mean and standard deviation can be calculated.

When enough samples are measured, the normal distribution of the samples can nearly replace the overall normal distribution. Thus, this study uses the MCM method, with the limited measurement distribution parameters as the input, and sets enough analogue samples M to predict the final measurement results [18,19]. The MCM method calculation process is as follows:

Step 1. Modeling. Based on the requested problem, construct a model, determine the model's input variables, and set a probability statistical distribution model for the variables.

Step 2. Random sampling. Based on the previous model, conduct a large sample sampling of the input variables.

Step 3. Estimation. Conduct simulation experiments on the model, set the number of simulations M, and calculate the output distribution of the model through the cyclic operation.

The calculation idea is shown in Fig. 5.

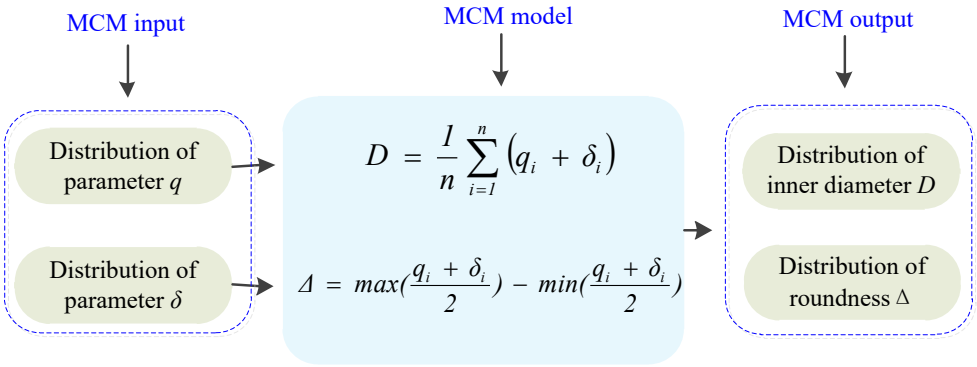


Fig. 5. Evaluate measurement values using MCM method

## 3. Experiment and analysis

The pneumatic inner diameter detection method replaces manual detection in the mechanical manufacturing process with high accuracy and low-cost advantages. Strict environmental control is not carried out during the experimental design to adapt to the complex detection environment of industrial sites. The experimental system is installed without constant temperature and vibration isolation, and the tested parts are bonded and assembled with the rotating table to meet multi-angle measurements. The overall system is shown in Fig. 6.

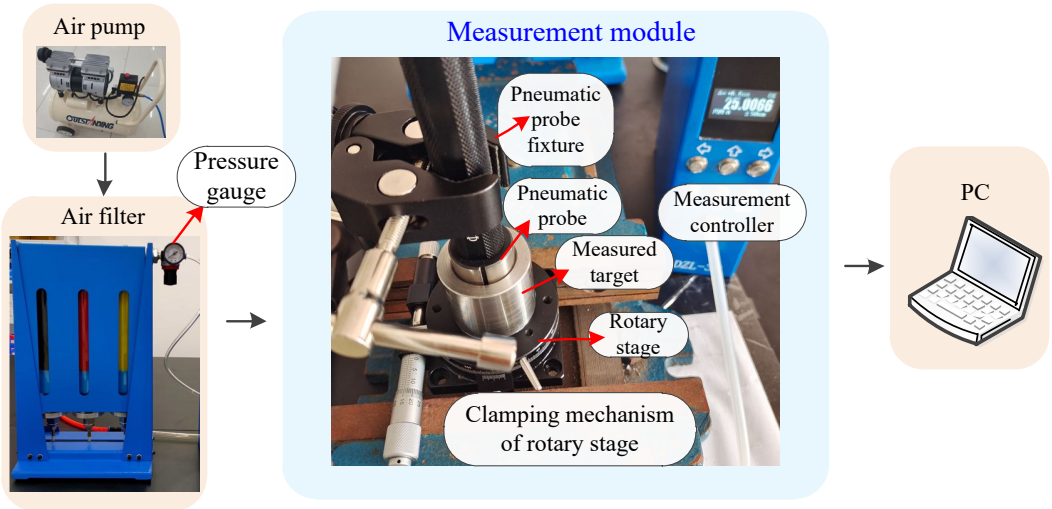


Fig. 6. Experimental System Structure

Type of the instrument is DZL-3D, from San Men Xia Zhong Xing precision measure CO., LTD. Henan, China. Instrument parameters are provided by the manufacturer. The instrument has four display ranges of 10μm, 20μm, 50μm, and 100μm, with corresponding display resolutions of 0.1μm, 0.2μm, 0.5μm, and

1.0μm, respectively. In addition, the input air pressure range is 0.40~0.75MPa. An uninterrupted purified gas supply was used in the experiment, with a pressure not less than 0.40 MPa, which can be observed from the pressure gauge on the air filter. In order to ensure safety, the air pressure is not set to exceed 0.50 MPa. The air pressure can be flexibly selected within the range of 0.40~0.75MPa, thus we have not set the independent air pressure monitoring module in this study. The initial output display resolution can be selected on the controller. If the measured size changes beyond the current display range, the instrument will automatically adjust the resolution to match the new measurement range. Thus, the output display resolution was set to 0.1μm at the beginning of the experiment. The measured value is automatically output on the instrument's built-in display screen. In the experiment, a RS-232 serial port is used to connect the instrument and computer to read the measurement data. All the data in this study are obtained through this method. The repeatability of a single point is measured, as shown in Fig. 7.

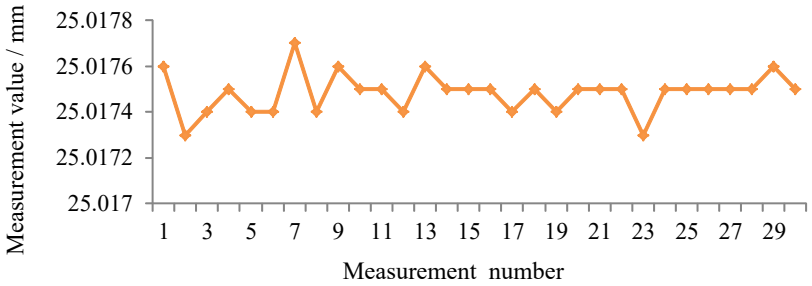


Fig. 7. Repeatability of a single point

Figure 7 shows 30 measurement points, with an interval of approximately 1 minute between each point. The standard deviation calculated using the Bessel formula is about 0.0001 mm, demonstrating good single-point repeatability.

According to the aforementioned error analysis principle, three sets of different starting angles were designed to measure a cylinder's inner diameter at the same height: 0°, 3° and 6°. The equally spaced measurement angles were 10°, and each group measured 18 positions on the circumference, with 5 measurements to verify the effectiveness of the repeated experiment. Roundness is a long-period error, so angle positioning using a rotary table can meet the measurement accuracy. The measurement results are shown in Fig. 8.

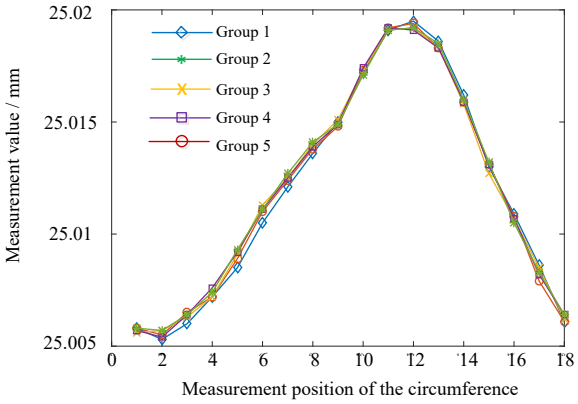


(a) Repetitive measurement results at 0 ° position

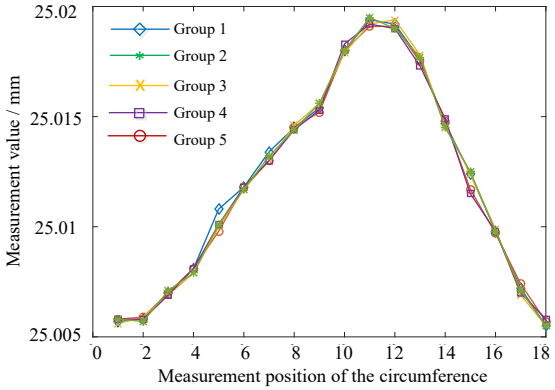


(b) Repetitive measurement results at 3 ° position

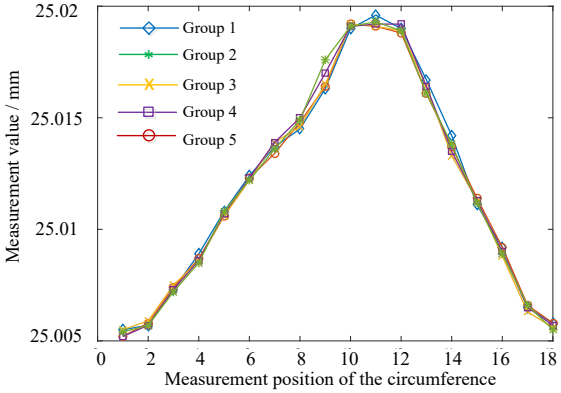


(c) Repetitive measurement results at 6 ° position

Fig. 8. Repeated measurement results at multiple angles of parts

The minimum value obtained from 5 measurements of 18 measurement positions at each angle is subtracted from the maximum value to obtain the repeatability range $v_i$ distribution, which is the extreme difference, as shown in Fig. 9.

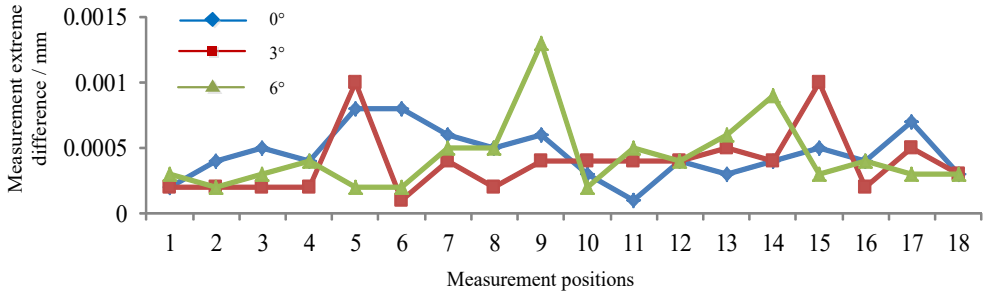


Fig. 9. Measurement repeatability of multiple angles

It should be noted that the 18 absolute measurement positions of the three groups in Figure 9 do not coincide on the circumference, and are only used to visually display the range distribution of the 18 positions in each group. The average range of repeated measurements at each position in Figure 9 is 0.0007 mm, showing good repeatability. Given the extremely low repeatability of the single point measurement in Figure 7, the multiple sets of repeatability errors in Figure 9 are the radial errors caused by the measurement line position in Figure 4. If an error $e$ is consistent with uniform distribution $U1(0, \max(e_i))$, the difference of any two $e_i$ is calculated, which can be any value between $-\max(e_i)$ and $\max(e_i)$, and also conforms to the uniform distribution. Therefore, the absolute value of the uniform distribution $U2$ is taken, which can replace $U1$. To consider extreme cases under limited measurement times and ensure accuracy, the radial error $\delta_i$ is replaced by the absolute value of the distribution of range $v_i$ in Figure 9. According to the central extreme value theorem, the sum $(v_i)$ is obtained by summing $v_i$ at 0°, 3° and 6° measuring positions, which conforms to the normal distribution, and its parameters are calculated to $\text{sum}(v_i) \sim N(0.00127, 0.00044^2)$. The radial errors of the three angles are similar, so sum $(v_i)$ is evenly distributed among the measurement results of the three angles. According to the normal distribution rule, 1/3 of sum $(v_i)$ is taken, that is, distribution $N(0.00043, 0.00015^2)$ as the estimated normal distribution of the error $\delta_i$ at each angle. $\delta_i$ is substituted into Equations (5) and (6) and then combined with the MCM method to predict the distribution of the inner diameter and roundness. The first data group is taken at the 0° measuring position, the MCM analogue number M is set to 10e5, and the circle's calculated inner diameter and roundness distribution are shown in Fig. 10.

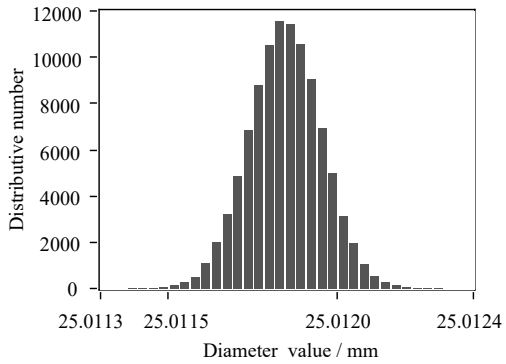


(a) Diameter distribution at 0 °

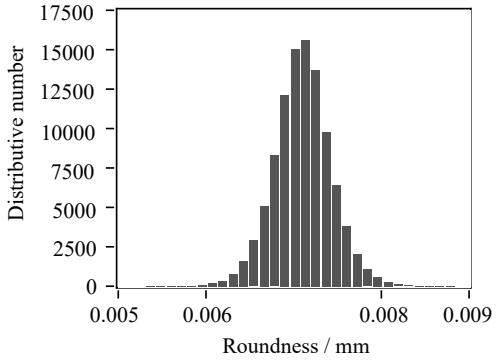


(b) Roundness distribution at 0 °

Fig. 10. Evaluation of hole parameters at 0 °using MCM

According to the calculated distribution, the diameter is 25.0118 mm, and the standard uncertainty is 0.11 μm. The roundness is 7.10 μm, and the standard uncertainty is 0.32 μm. When the confidence probability is about 95%, take the inclusion factor $k$ as 2, the extended uncertainty of diameter is 0.22 μm. The extended uncertainty of roundness is 0.64 μm. The first set of data is taken from 3° and 6° measurement positions separately, and the results are calculated using MCM, as shown in Table 1.

*Table 1*

**Uncertainty evaluation results of in inner diameter and roundness**

| | Diameter(mm) | Standard uncertainty (μm) | Extended Uncertainty (μm) | Roundness(μm) | Standard uncertainty (μm) | Extended Uncertainty (μm) |
|---|---|---|---|---|---|---|
| 0° | 25.0118 | 0.11 | 0.22 | 7.10 | 0.32 | 0.64 |
| 3° | 25.0120 | 0.11 | 0.22 | 6.85 | 0.33 | 0.66 |
| 6° | 25.0120 | 0.11 | 0.22 | 7.05 | 0.32 | 0.64 |

The uncertainty evaluation results for the three positions in Table 1 are consistent, verifying the method's stability. Given the average effect, the uncertainty in calculating the inner diameter is relatively small. The measurement

value of roundness uncertainty is relatively large, and the uncertainty caused by radial error is approximately 9% of the roundness. Thus, the influence of radial error on roundness cannot be ignored, indicating the application significance of this evaluation method.

The pneumatic probe is customized according to the size of the tested part. The inner hole in this study is processed by a CNC machine tool. The diameters of the probe and the inner hole in Figure 2 are consistent at millimeter or even sub millimeter level. Therefore, the $k_i$ in Figure 4 is relatively small, resulting in a smaller radial error $\delta_i$, which has reached the submicron level in this study. When the method is used in industrial sites, the value of radial error will vary depending on the morphology accuracy of the tested part.

## 4. Discussion

This article uses statistical laws and MCM methods to predict the radial error that significantly impact the measurement parameters of the inner hole. However, the axial error of the probe is not considered, which is caused by the non-parallelism of the probe axis centerline with the inner hole axis. The error is shown in Fig. 11. The cylindrical probe is projected as a rectangle in the direction shown in the figure, with dimensions $a$ and $b$ on both sides. The angle between the probe and the measured hole wall is $\theta$. The actual measured value $l_i$ includes the error caused by the $\theta$. The axial theoretical measurement value is $qi=li*cos(\theta)$. $\theta$ is calculated from the following equation:

$$cos(\theta) = \frac{b}{\sqrt{(l_i - a)^2 + b^2}} \tag{7}$$

Given the unknown of $a$ and $b$, determining $q_i$ solely through $l_i$ is difficult. On the other hand, the premise for establishing Formula (7) is that the measuring head fully enters the interior of the part for measurement, which is difficult to achieve fully in engineering. In the actual measurement, the inner hole part only needs to cover the air outlet of the measuring probe in Fig. 11.

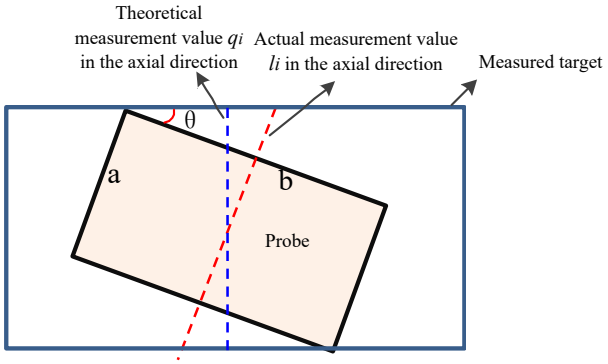


Fig. 11. Schematic diagram of measurement error in the axial direction

To determine the impact of axial error, the measurement results of the factory-calibrated ring gauge were used for evaluation. The pneumatic inner diameter measuring instrument adopts the pressure difference comparison method, and two calibration ring gauges are configured according to the tolerance of the measured parts. This study measures the inner hole part with a size of 25 ± 0.03 mm. Therefore, the upper and lower limit ring gauges verified by the manufacturer are configured as the measurement reference, as shown in Fig. 12. The inner diameters are 25.0290 and 24.9690 mm, respectively.


Fig. 12. Calibration ring gauges

The repeated measurement results of the two ring gauges using the measuring instrument are as follows:

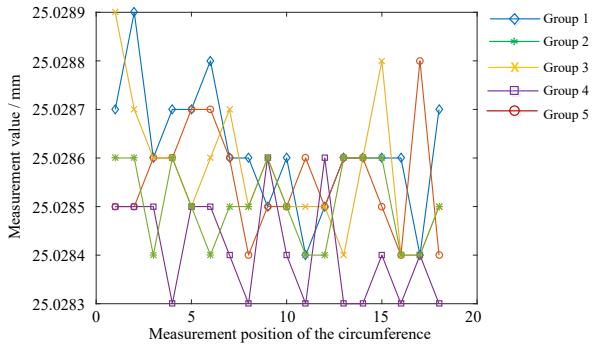


(a) Measurement result of upper limit ring gauges

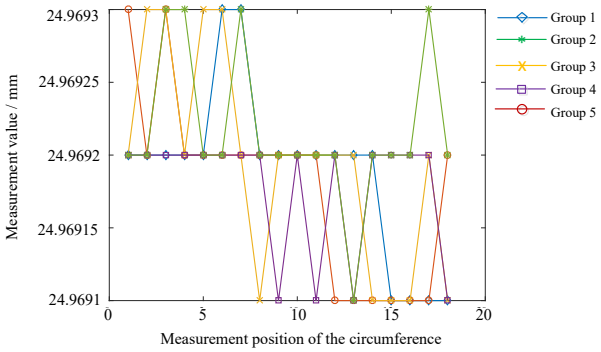


(b) Measurement result of lower limit ring gauges

Fig. 13. Measurement results of ring gauges

The average inner diameter of the upper limit ring gauge in Fig. 13 is 25.0286 mm, with a standard deviation of 0.00012 mm. The average inner diameter of the lower limit ring gauge is 24.9692 mm, with a standard deviation of (5.9e-5) mm. Both show good repeatability and are close to the nominal size calibrated in the factory. When the part size is within the upper and lower limits and the part and measuring probe are clamped stably, the axial error of the measuring probe has a minimal impact on the results, and its impact can be ignored. However, if the clamping mechanism is unstable, the impact of axial error may be significant. This error will be a complex dynamic error, and will be studied in future research.

When evaluating measurement uncertainty using the MCM method, the evaluation results are based on the current measurement as the reference for sample calculation, reflecting the current status. To improve the accuracy of measurement result evaluation, the Bayesian method [20,21] can be used to fuse the distribution of the current and pre-measurement samples for uncertainty evaluation, which will be the future research content.

## 5. Conclusion

A three-position pneumatic measurement method is presented to precisely measure the parameters of inner hole. The radial principle error is evaluated based on central extreme value theorem, and the uncertainties of the inner diameter and roundness are evaluated by using the Monte Carlo method (MCM). The inner hole diameter is 25.0118 mm ±0.22 μm($k$=2), and its roundness is 7.10 μm ± 0.64 μm($k$=2). Two factory-calibrated ring gauges are measured for evaluating the measurement accuracy, and the results showed that the method proposed is accurate and stable. Due to structural limitation, axial error is not considered in this study. The axial error correction method and more reliable uncertainty evaluation strategy will be further studied in next research.

## Acknowledgements

This work was supported by the Excellent Young Research Project of Anhui Provincial Department of Education's University Research Program (NO: 2022AH030160) and the Research Project of Anhui Institute of Information Technology (NO: rckj2021A005).

## REFERENCES

[1]. *Wozniak. A*, *Krajewski*. G and Byszewski. M, "A new method for examining the dynamic performance of coordinate measuring machines", in Measurement, **vol. 134**, Feb. 2019, pp.814-819

[2]. *Budisky*. R, *Kralik. M* and *Kost. J*, "Evaluation of True Position Using Coordinate Measuring Machine", in Applied Mechanics and Materials, **vol. 555**, Jun. 2014, pp. 511-517

[3]. *Kawalec*. *A* and *Magdziak*. *M*, "Usability assessment of selected methods of optimization for some measurement task in coordinate measurement technique", in Measurement, **vol. 45**, no. 10, Dec. 2012, pp. 2330-2338
[4]. *Kochetkov*. *A*. *V*, *Troshin*. *A*. *A*. and *Zakharov*. *O*. *V*, "Surface Texture Measurement with Profile Method Using Six-Axis Coordinate Measuring Machine", in Defect and Diffusion Forum, **vol. 410**, Aug. 2021, pp. 872-877
[5]. *Zeng. ZJ*, *Gao. GB* and *Ma. WJ*, "A Multi-Point Calibration Method of Articulated Arm Coordinate Measuring Machine", in Electronic Science and Technology, **vol. 35**, no. 08, 2022, pp. 73-78
[6]. *Ibaraki*. *S* and *Tanizawa*. *Y*, "Vision-Based Measurement of Two-Dimensional Positioning Errors of Machine Tools", in Journal of Advanced Mechanical Design Systems and Manufacturing, **vol. 5**, no. 4, 2011, pp. 315-328
[7]. *Min*. *J*, "Measurement method of screw thread geometric error based on machine vision", in Measurement & Control, **vol. 51**, no. 7-8, Sep-oct. 2018, pp. 304-310
[8]. *Wang*. *Y*, "Lateral distance measurement technology of driverless vehicle based on machine vision", in Journal of Computational Methods in Sciences and Engineering, **vol. 22**, no. 4, 2022, pp. 1373-1384
[9]. *Wen*. *X*, *Wang*. *JP*, *Zhang*. *GY* and *Niu*. *LQ*, "Three-Dimensional Morphology and Size Measurement of High-Temperature Metal Components Based on Machine Vision Technology: A Review", in Sensors, **vol. 21**, no. 14, Jul. 2021.
[10]. *Wu*. *FP*, *Zhu*. *SK* and *Ye*. *WL*, "A Single Image 3D Reconstruction Method Based on a Novel Monocular Vision System", in Sensors, **vol. 20**, no. 24, Dec. 2020.
[11]. *Feng*. *YY*, *Yang*. *T* and *Niu*. *YF*, "Subpixel Computer Vision Detection Based on Wavelet Transform", in IEEE Access, **vol. 8**, 2020, pp. 88273-88281
[12]. *Pieter*. *V*, *Rik*. *P* and *Guy*. *V*, "Robust beam width estimation with sub-pixel resolution in uncontrolled imaging conditions", in Applied Optics, **vol. 61**, no. 36, Dec. 2022, pp. 10807-10818
[13]. *Li. J, Pandiella. SS, et al*, "An experimental technique for the analysis of slug flows in pneumatic pipelines using pressure measurements, **vol. 20**, 2002, pp. 283-303
[14]. *Jamroz*. *BF* and *Williams*. *DF*, "Consistency in Monte Carlo Uncertainty Analyses", in Metrologia, **vol. 57**, no. 6, Dec. 2020
[15]. *Willink*. *R*, "On using the Monte Carlo method to calculate uncertainty intervals", in Metrologia, **vol. 43**, no. 6, Dec. 2006, pp. L39-L42
[16]. *Lee*. *JY* and *Kim*. *JK*, "A new propagation analysis of statistical uncertainty in multi-group cross sections generated by Monte Carlo method", in Annals of Nuclear Energy, **vol. 120**, Oct. 2018, pp. 477-484
[17]. *Fang. CZ, Huang. QX, et al*, "Measurement and uncertainty evaluation of the microsphere used for micro-CMM probe", in Measurement Science and Technology, **vol.31**.no.2, Feb.2020
[18]. *Papadopoulos*. *CE* and *Yeung*. *H*, "Uncertainty estimation and Monte Carlo simulation method", in Flow Measurement and Instrumentation, **vol. 12**, no. 4, Aug. 2001, pp. 291-298
[19]. *Cox*. *M*, *Harris*. *P* and *Siebert*. *RL*, "Evaluation of measurement uncertainty based on the propagation of distributions using Monte Carlo simulation", in Measurement Techniques, **vol. 46**, no. 9, Sep. 2003, pp. 824-833.
[20]. *Sankararaman*. *S* and *Mahadevan*. *S*, "Bayesian methodology for diagnosis uncertainty quantification and health monitoring", in Structural Control & Health Monitoring, **vol. 20**, no. 1, Jan. 2013, pp. 88-106
[21]. *Haruna*. *T*, "Uncertainty of the second order Quasispecies model with inverse Bayesian inference", in Artificial Life and Robotics, **vol. 24**, no. 3, Sep. 2019, pp. 297-303